ISSN 2075-1133, Inorganic Materials: Applied Research, 2021, Vol. 12, No. 6, pp. 1540–1546. © Pleiades Publishing, Ltd., 2021.
Russian Text © The Author(s), 2020, published in Voprosy Materialovedeniya, 2020, No. 3(103), pp. 17–28.

Strengthening Mechanisms of Rail Metal during Continuous Operation

V. E. Gromov[a, *], V. E. Kormyshev[a], Yu. F. Ivanov[b], A. A. Yuriev[c], A. M. Glezer[d], and Yu. A. Rubannikova[b]

[a] *Siberian State Industrial University, Novokuznetsk, 654007 Russia*
[b] *Institute of High Current Electronics , Siberian Branch, Russian Academy of Sciences, Tomsk, 634055 Russia*
[c] *AO EVRAZ Consolidated West Siberian Metallurgical Plant, Novokuznetsk, 654043 Russia*
[d] *Institute of Metal Science and Physics, Bardin Central Research Institute of Iron and Steel Industry, Moscow, 105005 Russia*
**e-mail: gromov@physics.sibsiu.ru*

Received July 24, 2020; revised August 28, 2020; accepted August 31, 2020

Abstract—A quantitative comparative analysis of the strengthening mechanisms for the surface layers of rails is carried out. It is based on the regularities in forming structure, phase composition, defective substructure, and properties of differentially hardened 100-m rails at different depths (up to 10 mm) and performed in the rail head along the central axis and along the symmetry axis of the fillet in the initial state and after various periods of extreme operation (with the handled tonnage of 691.8 and 1411 million gross tons). These regularities are identified using the methods of modern physical materials science. Contributions to strengthening due to friction of the matrix lattice, intraphase boundaries, dislocation substructure, the presence of carbide particles, internal stress fields, and solid solution strengthening of the pearlite constituent in the steel structure are assessed.

Keywords: strengthening mechanism, structure, phase composition, rails, operation

DOI: 10.1134/S2075113321060034

INTRODUCTION

The processes involved in the formation and evolution of structural-phase states and properties of rail surface layers during continuous operation pose a complex set of interrelated scientific and technical issues. The value of information in this area is linked to a thorough understanding of the fundamental problems of condensed matter physics, on one hand, and the practical significance of the problem, on the other hand [1, 2].

Recently, there has been a significant amount of interest in studying the condition of rails during continuous operation and analyzing the reasons for their removal. The expansion of information in this area is related both to the drive for understanding the fundamental problems of physical materials science and to the practical significance defined by the continuous increase in the requirements for rail reliability under present-day conditions of high axle loads and movement speeds.

The data bank on the regularities of formation of structural-phase states and dislocation substructure and distribution of carbon atoms in the head of long-length differentially hardened rails along the central axis and along the symmetry axis of the fillet was created for the initial state (preoperational condition) and intermediate tests (with the handled tonnage of 691.8 million gross tons) in [3, 4].

In recent years, the scientific literature has elaborated on the issues related to strengthening and wear of rails. Evidence has shown that wear defects are initially created in the surface layers. In addition, the constant wear initiation corresponds to the accumulation of plastic deformation reaching a certain level [5–10].

Creating the high-performance characteristics of rails should be based on the knowledge about mechanisms of structural phase changes in their section during continuous operation. These mechanisms can only be identified through the analysis of the evolution regularities of fine-structure parameters and the assessment of contributions of structural components and defective substructure to strengthening the rails during continuous operation.

The aim of this paper is to carry out a comparative analysis of the structural-phase state and the physical nature of metal strengthening in differentially hardened rails after megaplastic deformation under field conditions (with the handled tonnage of 691.8 and 1411 million gross tons).

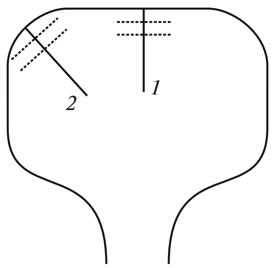

Fig. 1. Schematic diagram of the preparation of a rail sample through study of its structure using transmission electron diffraction microscopy. Solid lines indicate the directions along the central axis (*1*) and along the fillet (*2*); dotted lines indicate the locations of the metal layers used to prepare the foils (surface, 2 and 10 mm from the surface).

MATERIALS AND METHODS

The test materials were three batches of samples consisting of R65 rails of DT350 category. These samples were made of E76KhF steel and produced by AO EVRAZ Consolidated West Siberian Metallurgical Plant in May 2013 according to TU (technical specifications) 0921-276-01124323-2012. They were differentially heat-strengthened. The first batch consisted of samples in the initial state (before laying at the test site); the second batch consisted samples after the handled tonnage of 691.8 million tons gross during field tests at the test loop of the Railway Research Institute (AO VNIIZhT); and the third batch consisted samples after the handled tonnage of 1411 million gross tons.

According to the content of all chemical elements, the metal from all three batches satisfies the requirements of GOST R 51685-2013 for E76KhF steel (0.72% C; 0.77% Mn; 0.61% Si; 0.01% P; 0.01% S; 0.42% Cr; 0.07% N; 0.14% C; 0.04% V; 0.003% Al; and 0.003% Ti).

The studies of steel structure was carried out in much the same way as in [11] using optical microscopy methods (μVizo–MET-221P metallographic microvisor), scanning electron microscopy (Tescan MIRA3), X-ray structure analysis (Shimadzu XRD-7000S X-ray diffractometer, Japan), and transmission electron diffraction microscopy (EM-125).

The objects of study for transmission electron microscopy (foils ranging in thickness from 150 to 200 nm) were produced by electrolytic thinning of plates. They were located at the roll and fillet surfaces 2 and 10 mm from the surface and cut out using electrospark erosion of metal. The schematic diagram of the sample preparation is given in Fig. 1.

RESULTS AND DISCUSSION

Structural-Phase State of the Rail Metal in the Initial Condition

Differential hardening, or differential quenching, results in the formation of a polycrystalline structure composed of lamellar pearlite grains (Fig. 2a), degenerated pearlite grains (ferrite-carbide mixture) (Fig. 2b and 2c), and structurally free ferrite grains (ferrite grains without cementite particles). The main constituent of steel is lamellar pearlite. The relative amount of structurally free ferrite grains is low and varies from 0.01 to 0.05. The relative amount of lamellar pearlite grains along the central axis of the rails varies from 0.7 to 0.84 reaching a maximum at a depth of 2 mm. The relative amount of lamellar pearlite grains along the symmetry axis of the fillet varies from 0.61 to 0.73, reaching a maximum at a depth of 10 mm. The relative amount of degenerated perlite grains varies accordingly.

The lamellar pearlite dispersion (an interlamellar spacing value) depends on the distance to the head surface. The average value of interlamellar spacing at a depth of 2 and 10 mm is practically independent of the direction of studies (along the symmetry axis of the fillet or along the central axis) and its range is found to be 130–140 nm. The average interlamellar spacing in the layer forming the roll surface is 160 nm. In the layer forming the fillet surface, it is 185 nm.

The scalar dislocation density is essentially independent of the distance to the railhead surface. It varies within (4.0–4.6) × 10^{10} cm^{-2} in the lamellar pearl-

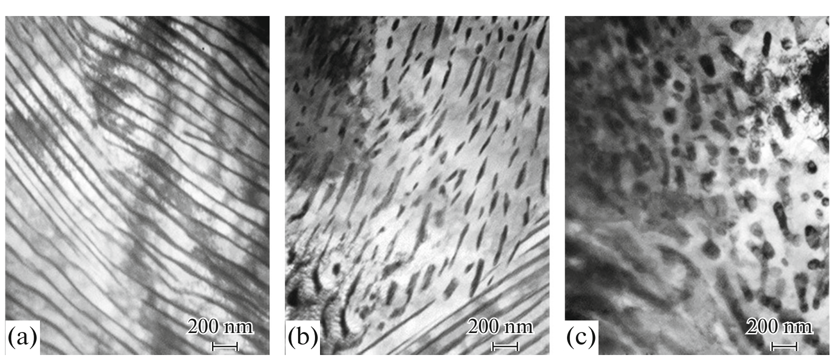

Fig. 2. Electron microscope images of lamellar pearlite grains (a) and degenerated pearlite grains (ferrite–carbide mixture) (b, c).

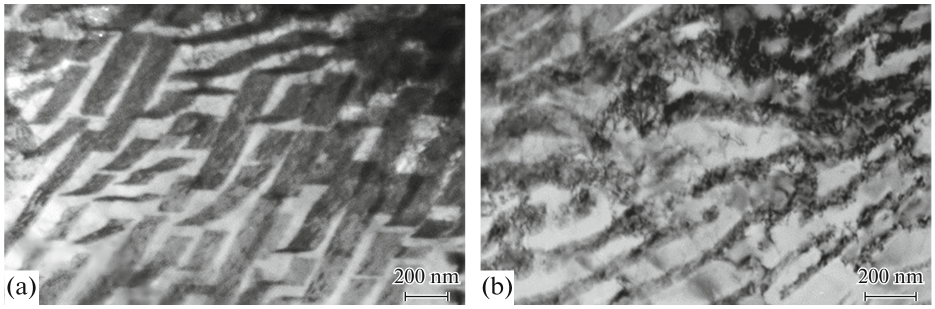

Fig. 3. Electron microscope images of a lamellar pearlite colony after the handled tonnage of 1411 million gross tons (a) and 691.8 million gross tons (b).

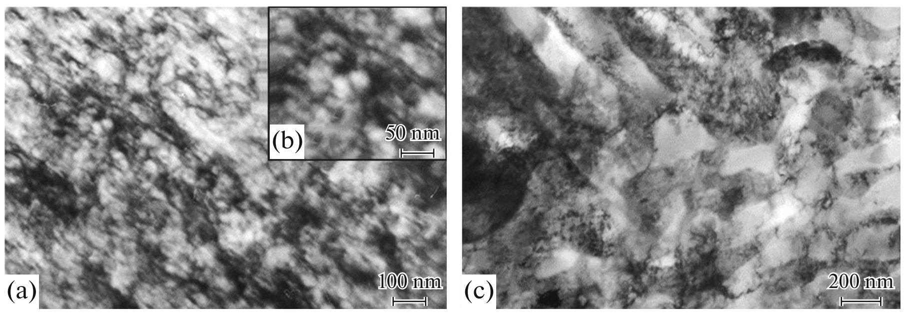

Fig. 4. Electron microscope images of the structure forming in the surface layer of the fillet (a, b) and the roll surface (c) after the handled tonnage of 1411 million gross tons.

ite grains and within $(5.0–6.0) \times 10^{10}$ cm^{-2} in the degenerated pearlite grains. The excess dislocation density varies within $(2.7–3.4) \times 10^{10}$ cm^{-2} in the lamellar pearlite grains and within $(3.8–5.2) \times 10^{10}$ cm^{-2} in the degenerated pearlite grains and decreases with distance from the head surface.

Structural-Phase State of the Rail Metal after the Handled Tonnage of 691.8 and 1411 Million Gross Tons

The plastic deformation occurring in metal during continuous operation of rails is mostly accompanied by the structure transformation in lamellar pearlite. Moreover, two concomitant processes of transformation of the structure and phase composition in lamellar pearlite colonies were observed to occur: firstly, cutting the cementite plates and, secondly, dissolving the cementite plates.

The first process is carried out in accordance with the mechanism of cutting carbide particles and removing their fragments. It is accompanied only by the change in their linear dimensions and morphology (Fig. 3a).

This fracture mechanism of pearlite colonies can be observed in the surface layer of the railhead after the handled tonnage of 691.8 million gross tons, and fracture of cementite plates in pearlite colonies was found both in the surface layer of the railhead and at a distance of ~10 mm from it after the handled tonnage of 1411 million gross tons.

The second fracture process of cementite plates in pearlite colonies takes place via the transition of carbon atoms from the crystal lattice of cementite to dislocations, followed by the precipitation of nanosized particles in the carbide phase in the subboundaries and elements of the dislocation substructure. The micrograph presented in Fig. 3b illustrates one stage in the formation of a dislocation substructure around the cementite plates. The transformation of the steel structure is observed to a greater extent in the surface layer of the railhead.

The structure of the fillet surface layer, which is formed after the handled tonnage of 1411 million gross tons, is given in Figs. 4a and 4b; and Fig. 4c presents the structure of roll surfaces. In both cases, a submicrocrystalline and nanocrystalline subgrain (fragmented) structure is formed on the surface. The sizes of subgrains (fragments) vary within 30–40 nm in the layer that forms the fillet surface (Fig. 4b). The sizes of subgrains (fragments) vary within 150–300 nm in the layer forming the roll surface (Fig. 4c). The relative content of the subgrain (fragmented) structure is 0.25 in the fillet surface layer, and it is 0.15 in the roll surface layer.

The transformations of the steel structure observed will have the largest effect on the strength and plastic characteristics of the metal, in the end determining the product life cycle. The assessments of the strengthening mechanisms help identify the regularities that link the parameters of the structure and the strength characteristics of the material and reveal the physical nature of the process of evolution of these characteristics.

Physical Nature of Rail Metal Strengthening during Continuous Operation

The assessment of strengthening mechanisms was conducted using the well-known and thoroughly tested expressions described below.

The steel strength level (yield stress) due to the formation of lamellar pearlite can be assessed in accordance with the formula [12]

$$\sigma(\mathrm{P}) = k_{\mathrm{s}}(4.75L)^{-1/2}\,0.24V(\mathrm{P}), \tag{1}$$

where L is the spacing between cementite plates;

V(P) is the relative content of lamellar pearlite in steel;

k_s is the strengthening factor, $k_s = 2 \times 10^{-2}$ Pa m$^{1/2}$.

The stress required to maintain the plastic deformation, i.e., the flow stress σ required to overcome the forces of interaction with immobile dislocations ("forest" dislocations) through moving dislocations (deformation carriers), is related to the scalar dislocation density by the following relation [12]:

$$\sigma_{\mathrm{d}} = \sigma_0 + \alpha m G b\sqrt{\langle\rho\rangle}, \tag{2}$$

where σ_0 is the flow stress of nondislocation origin (i.e., it is caused by other strengthening mechanisms);

$\langle\rho\rangle$ is the average (scalar) dislocation density;

m is the Schmid orientation factor;

α is the parameter characterizing the value of interdislocation interactions equal to 0.1–0.51;

G is the shear modulus of steel (~80 GPa);

b is the Burgers vector of a dislocation (0.25 nm).

In terms of the orientation factor m, $m\alpha = 0.5$ is usually taken for steels.

The operation of rails is accompanied by the formation of internal stress fields in the steel.

The value of the plastic component of the internal stress fields can be assessed using the relation [13]

$$\sigma(\mathrm{pl.}) = m\alpha G b\sqrt{\rho_{\pm}}. \tag{3}$$

The value of the elastic component of the internal stress fields can be assessed using the relation [13]

$$\sigma(\mathrm{elas.}) = m\alpha G t\chi_{\mathrm{elas}}. \tag{4}$$

Here, t is the foil thickness taken for the calculations equal to 200 nm;

χ_{elas} is the elastic component of the crystal lattice curvature–torsion.

The operation of rails is accompanied by the process of dynamic aging in steel, which results in the formation of nanosized iron carbide particles in the material. The steel hardening assessments which take into account the presence of incoherent second-phase particles are carried out using the relation [13]

$$\sigma_{\mathrm{ch}} = M\frac{mG_m b}{2\pi(|\lambda - D|)}\Phi\ln\left(\left|\frac{\lambda - D}{4b}\right|\right), \tag{5}$$

where λ is the average spacing between particles;

D is the average particle size;

m is the orientation factor equal to 2.75 for BCC (body-centered cubic) materials;

Φ is the coefficient characterizing the type of dislocations interacting with particles ($\Phi = 1$ for a screw dislocation and $\Phi = (1 - \upsilon)^{-1}$ for an edge dislocation);

M is the parameter which takes into account the uneven distribution of particles in the matrix equal to 0.81–0.85.

The low-angle boundary strengthening of the material (substructural strengthening, fragment boundary strengthening) separating the fragments can be assessed using the formula [12, 15]

$$\sigma(L) = \sigma_0 + kL^{-m}, \tag{6}$$

where $m = 1$ or 0.5 [16];

L is the average fragment size;

σ_0 is the friction stress in the crystal lattice of the material (30 MPa).

The operation of rails is accompanied, as discussed above, by dissolution (fracture) of cementite. The carbon released in this process is involved in the formation of nanoparticles in secondary cementite, accumulates on defects of the structure, and gets into the interstitial sites in the crystal lattice of steel. The assessment of the solid solution strengthening of steel due to carbon atoms and other alloying elements was carried out using an empirical expression of the form [16, 17]

$$\sigma(\mathrm{ss}) = \sum_{i=1}^{m} k_i C_i, \tag{7}$$

where k_i is the strengthening factor of ferrite, which is the gain in the material yield strength when 1 wt % of the alloying element is dissolved in it; the value of the factor k_i for various elements is determined empirically. C_i is the concentration of an element dissolved in ferrite, wt %.

The overall yield strength of steel in the first approximation based on the additivity principle, which means the independent action of each of the strengthening mechanisms of the material, can be represented as the linear sum of the contributions of the individual strengthening mechanisms [12, 16–18]:

Table 1. Assessments of strengthening mechanisms in metal structure of the rails (the contributions are given in terms of the volume fraction of the structure having this strengthening mechanism)

Average parameters for material	Roll surface			Fillet		
	Distance from surface					
	10 mm	2 mm	0	10 mm	2 mm	0
Initial state						
$\Delta\sigma(\mathrm{P})$, MPa	146	145	95.8	157	129	103.6
$\Delta\sigma(L)$, MPa	0	0	56	0	0	23
$\Delta\sigma(\rho)$, MPa	203	206	223	201	208	223
$\Delta\sigma(h)$, MPa	168	169	199.5	185.7	171.9	197.8
$\Delta\sigma(\mathrm{cp})$, MPa	103	114.4	167.2	119.4	177.3	182
$\Delta\sigma(\mathrm{ss})$, MPa	11	11	11.8	11	11	11.8
$\sigma = \sum_{i=1}^{n} \sigma_i$, MPa	631	645.4	753	684	697	741.4
After handled tonnage of 691.8 million gross tons						
$\Delta\sigma(\mathrm{P})$, MPa	165	140	41	165	115	48
$\Delta\sigma(L)$, MPa	0	0	0	0	0	0
$\Delta\sigma(\rho)$, MPa	340	356	363	330	350	375
$\Delta\sigma(h)$, MPa	274	351	356	230	300	320
$\Delta\sigma(\mathrm{cp})$, MPa	0	0	113	0	0	67
$\Delta\sigma(\mathrm{ss})$, MPa	0	0	133	0	0	133
$\sigma = \sum_{i=1}^{n} \sigma_i$, MPa	779	847	1006	725	765	943
After handled tonnage of 1411 million gross tons						
$\Delta\sigma(\mathrm{P})$, MPa	142.5	161.5	85.5	152	152	95
$\Delta\sigma(L)$, MPa	0	0	473.3	0	0	1455.6
$\Delta\sigma(\rho)$, MPa	152.8	181	181.4	164	206	190.4
$\Delta\sigma(h)$, MPa	131.3	149	255	148.6	149.6	230.4
$\Delta\sigma(\mathrm{cp})$, MPa	154.1	148.5	107	80.6	222.9	195
$\Delta\sigma(\mathrm{ss})$, MPa	11	11	11.7	11	11	11.7
$\sigma = \sum_{i=1}^{n} \sigma_i$, MPa	591.7	651	1114	556.2	741.5	2178.1

$$\sigma = \Delta\sigma_0 + \Delta\sigma(L) + \Delta\sigma(\rho) + \Delta\sigma(h) + \Delta\sigma(\mathrm{cp}) + \Delta\sigma(\mathrm{ss}) + \Delta\sigma(\mathrm{P}), \quad (8)$$

where $\Delta\sigma_0$ is the contribution due to the matrix lattice friction equal to 30 MPa;

$\Delta\sigma(L)$ is the contribution due to intraphase boundaries;

$\Delta\sigma(\rho)$ is the contribution due to the dislocation substructure;

$\Delta\sigma(\mathrm{cp})$ is the contribution due to the presence of carbide phase particles;

$\Delta\sigma(h)$ is the contribution due to internal stress fields;

$\Delta\sigma(\mathrm{ss})$ is the contribution due to solid solution strengthening;

$\Delta\sigma(\mathrm{P})$ is the contribution due to the pearlite component of the steel structure.

Thus, having defined the quantitative characteristics of the steel structure, it is possible to carry out the analysis of the physical mechanisms responsible for the evolution of the steel yield strength during operation and also to identify the physical mechanisms for formation of the strength gradient in the rail steel.

From the quantitative analysis of the steel structure obtained earlier in [1–4, 19–21], as well as here, the mechanisms of steel strengthening were assessed. The assessments are shown in Table 1.

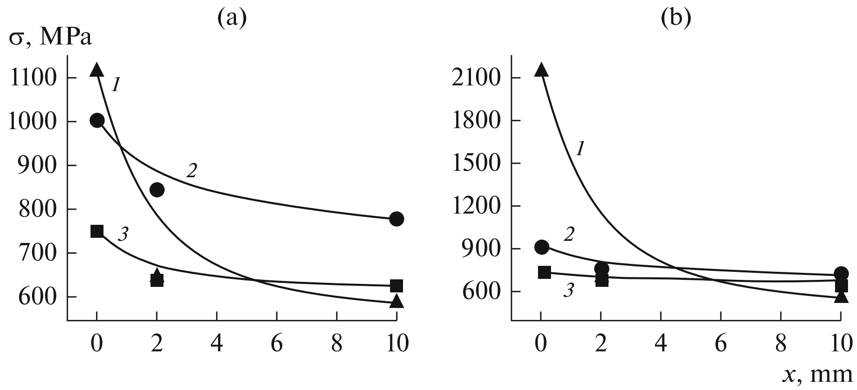

Fig. 5. Dependences of the total yield strength of steel on the distance to the railhead surface along the central axis (a) and along the symmetry axis of the fillet (b): (*1*) 1411 million tons; (*2*) 691.8 million tons; (*3*) initial state.

When analyzing the results shown in Table 1, we can note the following. Firstly, the steel strength is a multifactorial variable and is determined by the combined effect of some physical mechanisms. Secondly, the strength of the rail metal is dependent on the distance to the head surface, irrespective of the test point (along the central axis or along the symmetry axis of the fillet). Thirdly, the metal strength increases toward the head surface and it is higher along the symmetry axis of the fillet than along the central axis. Fourthly, the major strengthening mechanism of metals in the surface layer (in the layer forming the head surface) after the handled tonnage of 1411 million tons is substructural, which is due to the interaction of moving dislocations with small-angle boundaries of fragments and nanosized subgrains.

In Fig. 5, the dependences of the total yield strength of steel in the 100-m differentially hardened rails on the distance to the head allow monitoring of changes in the metal strength during operation. Here, it is clearly seen that the increase in the handled tonnage during operation in the range from 691.8 to 1411 million tons results in a significant increase (1.5–2 times) in the yield strength of steel. In addition, only the metal surface layer with a thickness of no more than 2 mm is subjected to strengthening. The strength characteristics of steel at greater distance from the head surface remain at the level of strength characteristics of steel in the initial state. The strength of the steel surface layer essentially is largely dependent on the location of the tested layer; namely, the strength of the metal surface layer in the fillet (Fig. 5b) is almost 2 times higher than the strength of the metal surface layer in the roll surface (Fig. 5a).

The plastic deformation of most metals and alloys is accompanied by fragmentation of the grain structure [22]. The evolution of the fragmentized structure that occurs when the degree of deformation increases results in the formation of local sites incapable of further evolution (a so-called critical structure is formed [22]). This critical structure acts as a point for the ductile fracture initiation of the material. On the basis of the results given in Table 1, it may be expected that the fracture of the metal will occur primarily in the surface layer of the fillet, where the formation of a subgrain structure with subgrain sizes of 100 nm after 1411 million tons is observed.

CONCLUSIONS

The plastic deformation of the metal during operation of rails is accompanied by the transformation of the structure in the lamellar pearlite colonies: firstly, by cutting the cementite plates and, secondly, by dissolving them. These fracture mechanisms of pearlite colonies can be found in the surface layer of the railhead up to 2 mm thick after the handled tonnage of 691.8 million gross tons. The fracture of cementite plates in the pearlite colonies after the handled tonnage of 1411 million gross tons is found in the layer ~10 mm thick. In addition, a submicrocrystalline and nanocrystalline subgrain (fragmentized) structure is formed in the surface layer of the railhead. The sizes of subgrains (fragments) in the layer forming the fillet surface vary between 30 and 40 nm. The sizes of subgrains (fragments) in the layer forming the roll surface vary between 150 and 300 nm. The relative content of the subgrain (fragmentized) structure is 0.25 in the surface layer of the fillet and 0.15 in the surface layer of the roll surface.

In particular, this paper presents the following results: (1) the steel strength is a multifactorial variable and is determined by the combined effect of some physical mechanisms; (2) the metal strength level increases toward the railhead surface; (3) the main strengthening mechanism of metals in the surface layer (in the layer forming the railhead surface) after the handled tonnage of 1411 million tons is the substructural mechanism, which is due to the interaction of moving dislocations with low-angle boundaries of fragments and subgrains; (4) the steel strength level (yield strength) increases greatly (1.5–2 times) with increasing handled tonnage in the range from 691.8 to 1411 million tons; and (5) the strength of the metal surface layer in the fillet is almost 2 times higher than the strength of the metal surface layer in the roll surface.

Therefore, the suggestion has been made that the fracture of the rail metal will occur primarily in the surface layer of the fillet, where the formation of local sites with the so-called critical structure incapable of further evolution has already been observed after the handled tonnage of 1411 million tons.

FUNDING

The study of the structural-phase state of steel was carried out with the financial support of a grant from the Russian Foundation for Basic Research (RFBR) in the framework of project no. 19-32-60001. The study of the strengthening mechanisms was carried out with the financial support of a grant from the Russian Science Foundation (RSF) in the framework of project no. 19-19-00183.

REFERENCES

1. Gromov, V.E., Peregudov, O.A., Ivanov, Yu.F., Konovalov, S.V., and Yuriev, A.A., *Evolyutsiya strukturno-fazovykh sostoyanii metalla rel'sov pri dlitel'noi ekspluatatsii* (Evolution of Structural-Phase States of Rail Metal in Long-Term Operation), Novosibirsk: Sib. Branch Russ. Acad. Sci., 2017.
2. Gromov, V.E., Ivanov, Yu.F., Yuriev, A.B., and Morozov, K.V., *Microstructure of Quenched Rails*, Cambridge: CISP, 2016.
3. Ivanov, Yu.F., Gromov, V.E., Yur'ev, A.A., et al., The nature of surface hardening of differentially hardened rails during long-term operation, *Deform. Razrush. Mater.*, 2018, no. 4, pp. 67–85.
4. Gromov, V.E., Yuriev, A.A., Ivanov, Yu.F., et al., Evolution of structure and properties of differentially quenched rails during long-term operation, *Metallofiz. Nov. Tekhnol.,* 2017, vol. 39, no. 12, pp. 1599–1646.
5. Ivanisenko, Yu. and Fecht, H.J., Microstructure modification in the surface layers of railway rails and wheels, *Steel Tech.,* 2008, vol. 3, no. 1, pp. 19–23.
6. Ivanisenko, Yu., Maclaren, I., Souvage, X., Valiev, R.Z., and Fecht, H.J., Shear-induced $\alpha \to \gamma$ transformation in nanoscale Fe–C composite, *Acta Mater.,* 2006, vol. 54, pp. 1659–1669.
7. Lewis, R., Christoforou, P., Wang, W.J., Beagles, A., Burstow, M., and Lewis, S.R., Investigation of the influence of rail hardness on the wear of rail and wheel materials under dry conditions (ICRI wear mapping project), *Wear*, 2019, vols. 430–431, pp. 383–392.
8. Skrypnyk, R., Ekh, M., Nielsen, J.C.O., and Pålsson, B.A., Prediction of plastic deformation and wear in railway crossings. Comparing the performance of two rail steel grades, *Wear,* 2019, vols. 428–429, pp. 302–314.
9. Kim, D., Quagliato, L., Park, D., and Kim, N., Lifetime prediction of linear slide rails based on surface abrasion and rolling contact fatigue-induced damage, *Wear*, 2019, vols. 420–421, pp. 184–194.
10. Huang, Y.B., Shi, L.B., Zhao, X.J., Cai, Z.B., Liu, Q.Y., and Wang, W.J., On the formation and damage mechanism of rolling contact fatigue surface cracks of wheel/rail under the dry condition, *Wear*, 2018, vols. 400–401, pp. 62–73.
11. Ivanov, Yu.F., Gromov, V.E., Kormyshev, V.E., and Glezer, A.M., Structure and properties of rails after extremely long-term operation, *Vopr. Materialoved.*, 2020, no. 2 (102), pp. 30–39.
12. Pickering, F.B., *Physical Metallurgy and the Design of Steels,* London: Appl. Sci., 1978.
13. Koneva, N.A., Kiseleva, S.F., and Popova, N.A., *Evolyutsiya struktury i vnutrennie polya napryazhenii. Austenitnaya stal'* (Structure Evolution and Internal Stress Fields. Austenitic Steel), Saarbrucken: LAP Lambert Acad., 2017.
14. Yao, M.J., Welsch, E., Ponge, D., Haghighat, S.M.H., Sandlöbes, S., Choi, P., Herbig, M., Bleskov, I., Hickel, T., Lipinska-Chwalek, M., Shantraj, P., Scheu, C., Zaefferer, S., Gault, B., and Raabe, D., Strengthening and strain hardening mechanisms in a precipitation-hardened high-Mn light weight steel, *Acta Mater.*, 2017, vol. 140, pp. 258–273.
15. Tushinskii, L.I., Bataev, A.A., and Tikhomirova, L.B., *Struktura perlita i konstruktivnaya prochnost' stali* (Pearlite Structure and Constructive Strength of Steel), Novosibirsk: Nauka, 1993.
16. Belen'kii, B.Z., Farber, B.M., and Gol'dshtein, M.I., Estimates of the strength of low-carbon low-alloy steels according to their structural data, *Fiz. Met. Metalloved.,* 1975, vol. 39, no. 3, pp. 403–409.
17. Sieurin, H., Zander, J., and Sandström, R., Modelling solid solution hardening in stainless steels, *Mater. Sci. Eng., A.*, 2006, vol. 415, pp. 66–71.
18. Prnka, T., Quantitative relations between parameters of disperse segregations and mechanical properties of steels, *Metalloved. Term. Obrab. Stali*, 1979, no. 7, pp. 3–8.
19. Kormyshev, V.E., Gromov, V.E., Ivanov, Yu.F., and Glezer, A.M., Structure of differentially hardened rails after severe plastic deformation, *Russ. Metall. (Metally)*, 2021, vol. 2021, pp. 426–429. https://doi.org/10.1134/S0036029521040169
20. Kormyshev, V.E., Gromov, V.E., Ivanov, Yu.F., Glezer, A.M., Yuriev, A.A., Semin, A.P., and Sundeev, R.V., Structural phase states and properties of rails after long-term operation, *Mater. Lett.*, 2020, vol. 268, art. ID 127499.
21. Kormyshev, V.E., Polevoi, E.V., Yur'ev, A.A., Gromov, V.E., and Ivanov, Yu.F., The structural formation in differentially-hardened 100-meter-long rails during long-term operation, *Steel Transl.*, 2020, vol. 50, no. 2, pp. 77–83. https://doi.org/10.3103/S0967091220020047
22. Rybin, V.V., *Bol'shie plasticheskie deformatsii i razrushenie metallov* (Large Plastic Deformations and Fracture of Metals), Moscow: Metallurgiya, 1986.

Translated by N. Bogacheva